HHS Public Access

Author manuscript

J Drug Target. Author manuscript; available in PMC 2016 May 08.

Published in final edited form as:

J Drug Target. 2015 ; 23(7-8): 736–749. doi:10.3109/1061186X.2015.1065833.

Systemic Delivery of Blood-Brain Barrier Targeted Polymeric Nanoparticles Enhances Delivery to Brain Tissue

Jennifer K. Saucier-Sawyer[1], **Yang Deng**[1], **Young-Eun Seo**[1], **Christopher J. Cheng**[1,2], **Junwei Zhang**[3], **Elias Quijano**[1], and **W. Mark Saltzman**[1]

[1]Department of Biomedical Engineering, Yale University, New Haven, CT, USA

[2]Department of Molecular, Cellular and Developmental Biology, Yale University, New Haven, CT, USA

[3]Department of Chemical Engineering, Yale University, New Haven, CT, USA

Abstract

Delivery of therapeutic agents to the central nervous system is a significant challenge, hindering progress in the treatment of diseases such as glioblastoma. Due to the presence of the blood-brain barrier (BBB), therapeutic agents do not readily transverse the brain endothelium to enter the parenchyma. Previous reports suggest that surface modification of polymer nanoparticles can improve their ability to cross the BBB, but it is unclear whether the observed enhancements in transport are large enough to enhance therapy. In this study, we synthesized two degradable polymer nanoparticle systems surface-modified with ligands previously suggested to improve BBB transport, and tested their ability to cross the BBB after intravenous injection in mice. All nanoparticle preparations were able to cross the BBB, although generally in low amounts (<0.5% of the injected dose), which was consistent with prior reports. One nanoparticle produced significantly higher brain uptake (~0.8% of the injected dose): a block copolymer of polylactic acid and hyperbranched polyglycerol, surface modified with adenosine (PLA-HPG-Ad). PLA-HPG-Ad nanoparticles provided controlled release of camptothecin, killing U87 glioma cells in culture. When administered intravenously in mice with intracranial U87 tumors, they failed to increase survival. These results suggest that enhancing nanoparticle transport across the BBB does not necessarily yield proportional pharmacological effects.

Keywords

Polymeric nanoparticles; blood-brain barrier; poly(lactic acid); poly(lactide-co-glycolide); DSPE-PEG; hyperbranched polyglycerol (HPG); adenosine

Address for correspondence: W. Mark Saltzman, Department of Biomedical Engineering, Yale University, Malone Engineering Center, 55 Prospect Street, New Haven, CT 06511 USA Tel: (203) 432-3281 mark.saltzman@yale.edu.

Declaration of interest The authors report no conflicts of interest.

Dedication

Robert Langer is the world's leading thinker and doer in the field of drug delivery and targeting. This paper describes an approach for using polymers to deliver drugs to the brain. Bob published the first paper showing that polymers could be used to deliver agents to targeted areas of the brain in 1981 (1). At about that time, he introduced one of us (WMS) to the potential value of novel drug delivery systems targeted to brain disease (2, 3). Bob's support and encouragement was pivotal in the directions our laboratory took in defining the role of polymers for delivery of chemotherapy agents to brain tumors (4, 5). It is with deep gratitude that we dedicate this paper to Bob, in honor of his receiving the 2015 Lifetime Achievement Award.

Introduction

Incidence of diseases affecting the central nervous system (CNS) is on the rise with projections estimating it will reach 14% of all global diseases by 2020 (6). Brain and CNS tumors are of particular concern, with more than 20,000 new cases diagnosed in 2014, resulting in over 14,000 deaths in the US alone (7). In particular, glioblastoma multiforme (GBM) is a highly aggressive, invasive, and deadly form of primary brain tumor. The current treatment for GBM involves surgical resection, if possible, followed by chemotherapy, typically with temozolomide, and radiation (8, 9). Even with this aggressive regimen, median survival for patients diagnosed with GBM is ~14 months and a cure for the disease remains elusive (10).

Compared to other peripheral tumors, brain and CNS tumors pose a unique hurdle for treatment. The blood-brain barrier (BBB) presents a significant challenge to the systemic delivery of therapeutic agents to the brain (11). This protective barrier is composed of a layer of brain endothelial cells supported by astrocytes and pericytes, which prevents movement of all but small lipophilic molecules between the blood and the brain extracellular fluid (12). Tight gap junctions, which limit paracellular transport through the monolayer of brain endothelial cells, are a primary characteristic of the BBB. The lack of transvascular access imposes a severe limitation on the treatment of neurological conditions such as brain tumors. Even in the presence of a brain tumor, the blood-tumor barrier remains mostly intact, reducing the enhanced permeability and retention effect (EPR) observed in peripheral tumors and limiting uptake of agents into the tumor environment (13, 14).

Due to their small size in relation to cells, nanoparticles (NPs) have been investigated as a potential means to enhance delivery of agents to the brain (15–18). Polymeric NPs offer the potential benefits of controlled release and protection of payloads from degradation. For example, poly(lactic-co-glycolic acid) (PLGA) and polylactic acid (PLA) are biodegradable polymers that have been approved by the FDA in drug delivery applications (19); NPs fabricated from PLGA or PLA have potential advantages over other delivery systems—such as liposomes and dendrimers—due to their inherent biodegradability (20), their lack of toxicity, and their ability to deliver hydrophilic compounds such as nucleic acids (21), hydrophobic agents such as camptothecin (CPT) (22), and drug/nucleic acid combinations (23, 24).

To have an impact on brain diseases, NPs must circulate and cross the BBB. Long circulation should enhance penetration of the BBB by allowing more time for NP transport. One of the most significant barriers to long circulation of polymer NPs is the body's natural response to injected particulates. In the blood, NPs can become coated with plasma proteins, in a process known as opsonization, which enhances their clearance by cells of the mononuclear phagocyte system (MPS) (20). As a result, injected NPs will be sequestered into phagocytic cells and transported to the spleen, liver, or lymph nodes before reaching target organs. Surface coating of polymeric NPs with poly(ethylene glycol) (PEG) has been shown to slow opsonization and MPS uptake, allowing the creation of “stealth” vehicles that exhibit prolonged circulation time (25–28). Significantly, PEG coatings also appear to enhance transport of NPs within the brain interstitium (29). Recently, our group developed a novel NP coating, hyperbranched polyglycerol (HPG), which has advantages over PEG, including enhanced surface coverage and prolonged circulation times (30).

In addition to the pharmacokinetic improvements imparted by stealth coatings, functionalizing NPs with targeting moieties can significantly improve BBB transport. Most approaches to enhance permeation of NPs through the BBB attempt to exploit transporters located on the luminal side of brain capillary endothelial cells (15, 31–33), although some NPs appear to be taken up by non-specific endocytosis, or absorptive endocytosis (34–36). Among transporters, receptors that are involved in receptor-mediated endocytosis, and capable of trafficking molecules into and through the cell (37)—such as receptors for insulin (38), transferrin (33), and low-density lipoprotein (39)—are of particular interest. Rabies virus glycoprotein (RVG), a 29 amino acid cell-penetrating peptide derived from an active targeting region of the rabies virus, has been found to specifically bind to the alpha subunit of the nicotinic acetylcholine receptor resulting in receptor-mediated transcytosis (40–42) and has been shown to be an effective targeting agent for certain particulates (42–45). TGN, a 12 amino acid peptide, was discovered through *in vivo* phage display in a mouse model. Although the uptake mechanism is unknown, PLGA NPs modified with TGN demonstrated increased uptake in the brain when compared to unmodified NPs (15). Finally, NPs conjugated with adenosine (Ad) have been recently explored by other groups (16, 46). Ad G-protein-coupled receptors, specifically A_{2A}, are found on brain endothelial cells, and reports have shown that this receptor can both increase uptake of therapeutic agents and modulate BBB permeability (16, 47, 48).

NPs encounter an additional transport barrier after they cross the BBB. Once in the brain parenchyma, NPs must move through the interstitial spaces of the brain and tumor (5), which are estimated to be less than 100 nm (49, 50). Production of NPs of small size (significantly less than 100 nm) enhances their ability to penetrate though the brain parenchyma and distribute within the tissue (5).

In this study, we selected three of the most promising BBB transport ligands (RVG, TGN and Ad) and synthesized NPs with these ligands attached to the surface of either PLGA with a PEGylated phospholipid linker (PLGA-DSPE-PEG) or PLA-HPG NPs of small diameter. We analyzed the properties of these NPs *in vivo* by measuring their accumulation in the brain of mice after intravenous injection. Finally, to examine the potential of our NPs to

deliver drugs to the brain, PLA-HPG NPs conjugated to Ad (PLAHPG-Ad), were loaded with CPT and tested for effectiveness by injection in mice with intracranial gliomas.

Materials and Methods

Materials

Ester-terminated poly(lactic-co glycolic acid) (PLGA, 50:50 copolymer ratio, 0.55–0.75 dL/g inherent viscosity) and Poly(DL-lactide) (PLA, 0.15–0.25 dL/g inherent viscosity) were acquired from LACTEL Absorbable Polymers, Durect Corporation (Birmingham, AL). Dichloromethane (DCM) was purchased from Fischer Scientific (Fair Lawn, NJ). Ethyl acetate and dimethyl sulfoxide (DMSO) were acquired from J.T. Baker (Center Valley, PA). 1,2-distearoyl-*sn*-glycero-3-phosphoethanolamine-N-[carboxy(polyethylene glycol)-2000] (DSPE-PEG) was purchased in the forms of DSPE-mPEG MW 2000 (DSPE-mPEG), DSPE-PEG-maleimide MW 2000 (DSPE-PEG), as well as DSPE-PEG-FITC MW 2000 (DSPE-PEG-FITC) from Nanocs (Boston, MA). coumarin 6, poly(vinyl alcohol) (PVA), trehalose, HEPES buffer, CPT, TWEEN 80, bovine serum albumin (BSA), Triton X-100, N,N-Dimethylformamide (DMF), N,N'-Diisopropylcarbodiimide (DIC), Trifluoroacetic acid (TFA), Hydrochloric acid solution (HCl), and heparin sodium salt were purchased from Sigma-Aldrich (St. Louis, MO). Paclitaxel was purchased from LC Laboratories (Woburn, MA). Phosphate buffered saline (PBS), penicillin-streptomycin (Pen-strep), nile red, Dulbecco's Modified Eagle Medium (DMEM) as well as Alexa Fluor 594 phalloidin dye were acquired from Life Technologies (Grand Island, NY). Fetal bovine serum (FBS) was purchased from Atlanta Biologicals (Flowery Bay, GA). U87 and bEnd.3 cells were obtained from American Type Tissue Culture (ATCC, Manassas, VA). 2',3'-Isopropylidene Adenosine-5'-carboxylic Acid was purchased from Santa Cruz (Dallas, TX). Snakeskin dialysis tubing (10K MWCO) and Bond-Breaker TCEP Solution were acquired from Thermo Scientific (Rockford, IL). EDTA was purchased from American Bioanalytical (Natick, MA). Custom synthesized peptides RVG (*YTIWMPENPRPGTPCDIFTNSRGKRASNG) and* RVMAT (MNLLRKIVKNRRDEDTQKSSPASAPLDDGC) were ordered from Keck Biotechnology Resource Laboratory (Yale University, New Haven, CT). Peptide TGN (TGNYKALHPHNGGGGGC) was fabricated by GenScript (Piscataway, NJ).

Synthesis of DSPE-PEG Ligand Conjugates

Peptide ligands were conjugated to DSPE-PEG as previously described (51). When noted, DSPE-mPEG as well as DSPE-PEG-FITC were unmodified and used as received. DSPE-PEG-RVG, DSPE-PEG-RVMAT, and DSPE-PEG TGN were fabricated through conjugation of the targeting ligand (RVG, RVMAT, TGN) to DSPE-PEG-maleimide via cysteine residues. Ligands were dissolved at 30 nM concentration in water and added to a buffer solution containing 100 mM HEPES and 10 mM EDTA with 50 mM TCEP at pH 7.5. After 1h, DSPE-PEG-maleimide at a 3X molar ratio was added to the peptide mixture and reacted overnight at room temperature. Dialysis was used to purify the conjugates. Conjugates were stored at 4°C until use.

PLGA-DSPE-PEG NP Fabrication

PLGA NPs were fabricated using a single emulsion solvent evaporation technique as described previously with minor modifications (5). PLGA was dissolved at 100 mg per ml in DCM overnight. Nile red (0.2% wt/wt) was dissolved in 1 ml ethyl acetate and added to the polymer solution immediately before fabrication. DSPE-PEG ligands, including those conjugated to peptides, were added to the aqueous phase (2 ml, 5% wt/vol PVA) before emulsion. DSPE-PEG-FITC NPs were fabricated at 1, 5, 10, and 15 nmol ligand per mg polymer while all other DSPE NPs were fabricated at 10 nmol ligand per mg polymer. The polymer phase was added dropwise to the aqueous phase under vortex and probe sonicated 3X for 30 s each before addition to 0.3% PVA solution under stirring for 4–5 hours to evaporate solvent. Particles were collected by centrifugation at 10,000 rpm where the supernatant was retained and washed 2X in DI water under ultracentrifugation at 24,000 rpm. NPs were resuspended in water with the addition of ~20% wt/wt trehalose as a cryoprotectant, flash frozen, lyophilized, and stored at −20°C until future use.

PLGA NP Characterization

Sizing, Morphology, and Zeta Potential—PLGA NPs were characterized for size and morphology using scanning electron microscopy (SEM) as well as sizing using dynamic light scattering (DLS). For SEM, dry NPs without trehalose were spread on carbon coated tape and gold sputter coated for 30 s under 40 mA current (Sputter Coated 180aute, Cressington). Samples were imaged in an XL-30 ESEM-FEG (FEI Company) under 10 kV acceleration voltage. ImageJ software (National Institutes of Health) was utilized to analyze the average size of the NPs. Sample populations of at least 1000 NPs were included for statistical analysis. For hydrodynamic sizing using DLS, NP samples were diluted to 0.05 mg/ml in DI water and read on a Malvern Nano-ZS and reported as Z-average diameter. To measure zeta potential, NPs were resuspended in DI water at a concentration of 0.5 mg/ml. 750 μl of solution was loaded into a disposable capillary cell (Malvern) and analyzed on a Malvern Nano-ZS.

Quantification of Ligand Surface Density—DSPE-PEG FITC was introduced during NP fabrication as described above to estimate the ligand incorporation and surface density via fluorescence. NPs were washed as described to remove any unincorporated ligand before lyophilization. After lyophilization, ~3mg of dry NPs were resuspended in 1 ml of DMSO and left at room temperature to dissolve for 1 h protected from light. 100 μl of NP solution was added to 900 μl of PBS to pH FITC for analysis. A standard curve of known molar concentrations of free DSPE-PEG-FITC ligand was created in identical buffer conditions. Samples were analyzed in triplicate in a 96 well black clear-bottom plate at ex/em 495/518 nm using a Molecular Devices SpectraMax M5 plate reader. The number of ligands per NP and surface density were approximated based on the assumption of spherical NPs of average size with a density of 1.2 g/cm^3 (52).

NP Loading—To quantify total loading of fluorophore, NPs loaded with nile red (ex/em 552/636) were directly dissolved in DMSO and quantified against a standard curve. Samples were read in a 96-well plate using a Molecular Devices SpectraMax M5 plate reader.

Fabrication and Characterization of PLA-HPG and PLA-HPG-Ad Polymers

Fabrication of PLA-HPG in our laboratory has been previously described in detail (30). To surface modify these NPs to create PLA-HPG-Ad, 500 mg PLA-HPG was added to 40 mg 2',3'-Isopropylidene Adenosine-5'-carboxylic Acid and dissolved in 12 ml anhydrous DMF. The solution was dried with molecular sieve with 39 μl DIC and 6 mg DMAP added to the solution. The reaction was slowly stirred for 2 days. To purify, the solution was centrifuged at 10,000 rpm for 10 min. The resulting supernatant was collected and added into a large amount of cold diethyl ether to precipitate the polymer. The polymer precipitate was collected by centrifugation at 10,000 rpm for 10 min. The resultant polymer was dissolved in 3 ml DCM/TFA mixture (DCM:TFA = 2:1) and the reaction was shaken at room temperature for 2 h. The resulting solution was added into a large amount of cold diethyl ether and the polymer was collected by centrifugation at 10,000 rpm for 10 min. The polymer was further purified by redissolving in DCM and precipitating in diethyl ether. The purified polymer was dried under vacuum for 2 days. To determine conjugation of Ad to PLA-HPG, PLA-HPG-Ad and PLA-HPG polymers were dissolved in DMSO-d6 and 1H NMR analysis was carried out on an Agilent DD2 400 MHz NMR Spectrometer. The average number of Ad per PLA was estimated based on the integral of peak 4 (6.35ppm) and peak 5 (5.18ppm)

Fabrication of PLA-HPG and PLA-HPG-Ad NPs

PLA-HPG and PLA-HPG-Ad NPs were fabricated using an emulsion solvent evaporation technique as described previously with slight modification (30). For nile red or coumarin 6 loaded PLA-HPG-NPs, 100 mg of PLA-HPG copolymer was dissolved in 2.4 ml ethyl acetate. Fluorophore was added to the polymer solution at 0.2% wt/wt in 0.6 ml DMSO. PLA-HPG-Ad NPs were fabricated by replacing a portion of PLA-HPG polymer with PLA-HPG-Ad modified polymer at 10, 5, or 1%. For CPT loaded NPs, CPT was dissolved at 5% wt/wt in 0.6 ml DMSO and added to the polymer/ethyl acetate mixture. To increase CPT loading, 20% wt/wt 16,000 MW free PLA was added to replace equal weight of PLA-HPG with other fabrication parameters remaining the same. The resulting polymer solutions were added to 4 ml of DI water under vortex and then probe sonicated 4X at 10 s each on ice. The resulting emulsion was suspended in 10 ml DI water under stirring. Ethyl acetate was evaporated using a rotary evaporator and the resulting solution transferred to an Amicon Ultracel 100K centrifugal filter unit. The NPs were washed 2X in DI water and then resuspended and frozen until use.

Characterization of PLA-HPG and PLA-HPG-Ad NPs

Sizing and Morphology—Particle characterization of PLA-HPG NPs was analyzed using both DLS and Transmission Electron Microscopy (TEM). DLS sizing and zeta potential was completed as described above. For TEM, a drop of NP suspension in DI water was placed on a carbon-coated copper grid. The NP droplet was allowed to dry for 10 min before application of a droplet of uranyl acetate. The sample was once again allowed to dry for 5 min and then mounted for imaging.

Loading of Drugs and Fluorophores—To quantify drug loading, CPT in NPs was assayed via fluorescence at ex/em 370/428 nm. NPs were dissolved in acidified DMSO containing 1% NP solution in water, 1% HCl (1N) and 98% DMSO. All samples and standards were diluted in a buffer solution at final concentrations of 1% HCl (1N), 1% DI water, and 98% DMSO. Free CPT was dissolved in buffer for use as a standard curve. Fluorescently loaded NPs (nile red and coumarin 6) were quantified as described above.

Controlled Release of CPT—Release from PLA-HPG and PLA-HPG-Ad NPs was performed under *in vitro* physiological conditions with triplicate samples. NPs suspended in water were placed in dialysis tubing (10K cut-off) under sink conditions in 40 ml of sterile PBS at 37°C with stirring. At designated timepoints, the dialyzate was reserved for analysis and replaced with 40 ml of fresh PBS. To quantify the amount of CPT released from the NPs, 970 μl of dilyzate from each sample and timepoint was added to 30 μl of acidified buffer (DMSO:10% SDS:1N HCl at a 1:1:1 volume ratio). The CPT concentration was detected using a Molecular Devices SpectraMax M5 plate reader at ex/em 370/428 and compared to NP loading to quantify total release.

In vivo delivery and quantification of fluorescent NP brain uptake

Mice were used to quantify brain uptake of fluorescently-labeled NPs. All animal procedures were performed in accordance with Yale IACUC protocols. Animals were kept in the Yale Animal Resource Center and given free access to food and water over the duration of the study. BALB/c mice (Charles River) were obtained at 8 weeks old. Nile red-loaded NPs were resuspended in PBS and administered at 200 mg/kg via the tail vein. At designated time points (PLGA-DSPE-PEG-RVG and PLGA-DSPE-PEG-RVMAT- 2 h, PLGA-DSPE-PEG-TGN – 4 h, PLA-HPG-Ad at 4 and 24 h), animals were sacrificed and immediately perfused with heparinized PBS to remove all blood. Brain tissue was carefully removed and washed with 1X PBS before placing in clean vials. Organs were frozen and lyophilized for 24 h to remove all aqueous matter. Tissues were resuspended in DMSO at 50 mg/ml concentrations and homogenized to extract fluorophores from the tissues. Tissue samples were centrifuged 2X at 15,000 rpm for 10 min to separate all tissue matter and debris from the DMSO sample. Nile red content in the samples was quantified in reference to a standard curve and background controls using a SpectraMax M5 plate reader at ex/em 552/636 nm. Percent dose was calculated based on the total injected dose of fluorophore in the NP samples with background PBS controls subtracted. Data was processed through an ordinary one-way ANOVA using Tukey's Multiple Comparisons Test to determine significance, which is denoted as * ($p \leq 0.05$), ** ($p \leq 0.01$), *** ($p \leq 0.001$).

In vitro cell culture and cellular assays

Immortalized mouse brain endothelial cells, bEnd.3, as well as U87 immortalized human glioblastoma cells were cultured in Dulbecco's Modified Eagle Medium (DMEM) supplemented with 10% fetal bovine serum and 1% penicillin-streptomycin. Cells were stored in a humidified incubator at 37°C under 5% CO_2.

Confocal Microscopy Analysis of NP internalization *in vitro*

bEnd.3 cells were plated on 1 cm sterile glass cover slips set in a 24-well tissue culture plate at a concentration of 1×10^3 cells per well and left over night to adhere. Glass cover slips were then transferred to a new tissue culture plate and coumarin 6 NPs were administered at a concentration of 0.2 mg/mL for either a 4 or 24 h period. Samples were washed 5X with PBS then fixed with 4% paraformaldehyde. Permeabilization of cells was completed with 0.1% Triton X (vol/vol) in a solution of 1% BSA (wt/vol) in PBS for 10 min. Cells were then incubated for membrane labeling with 1:40 dilution of Alexa Fluor phalloidin 594 in 1% BSA (wt/vol) in PBS for 20 min at room temperature and then rinsed 1X with PBS. Samples were mounted on glass slides for imaging using Vectashield mounting media (Vector Labs) with DAPI for nucleus staining. Cells were imaged on a Leica (Bannockburn, IL) TCS SP5 Spectral Confocal Microscope.

In vitro cytotoxicity of CPT-loaded NPs

To determine the *in vitro* cytotoxicity of both PLA-HPG and PLA-HPG-Ad CPT NPs, both bEnd.3 and U87 cells were plated in 96-well tissue culture plates at a density of 2×10^3 cells per well and left overnight to adhere. NPs as well as controls (Free drug and PBS) were diluted in DMEM at the highest specified concentration and serially diluted 1:10 in media. 100 μl of solution was added to each well. The cells were incubated for 72 h, at which point a Cell Titer Blue assay (Promega) was run to quantify cell viability for each treatment.

In vivo tumor implantation and survival analysis of U87 tumor-bearing mice injected with PLA-HPG-Ad NPs

Athymic nude mice (Charles River) were obtained at 8 weeks of age. Animals were housed in the Yale Animal Resource Center and all work was completed at Yale University in accordance with the Yale Institutional Animal Care and Use Committee (IACUC) guidelines. Mice were placed under ketamine (100 mg/kg) and xylazine (10 mg/kg) anesthesia with Meloxicam SR analgesia (5 mg/kg) until a surgical plane was achieved. Animals were placed in a stereotactic frame and their scalps sterilized with alternating betadine and alcohol administration. A mid-line incision was created and a 1mm burr hole was placed in the skull at 0.6 mm anterior, and 1.8 mm lateral to bregma in the right striatum. U87 cells, cultured as described above, were trypsinized, washed 2X in sterile saline and resuspended at a concentration of 10^8 cells per ml. A 10 μl Hamilton syringe loaded with cell solution was inserted into the burr hole at a depth of 3 mm and left to equilibrate for 5 min before infusion. A microinfusion pump was used to inject 2 μl of cell solution (2×10^5 cells per animal) at a rate of 1000 μl per min. The animal was left for 5 min for tissue equilibration to prevent backflow post infusion. Bone wax was used to fill the burr hole, and skin was stapled and cleaned. Animals were placed in a recovery cage until sternal.

To test the therapeutic benefit of our brain-targeted NPs, two survival studies were performed in these nude mice. In study 1, mice were administered either CPT-loaded PLA-HPG NPs (n=7), CPT-loaded PLA-HPG-Ad NPs (n=7), free CPT (suspended in a PBS solution with 10% vol/vol DMSO, 5% vol/vol Tween 80, and 85% vol/vol saline, n=6), or PBS (n=5) via the tail vein at 4 mg/kg CPT at days 3, 6, and 9 after intracranial infusion of tumor cells. In study 2, mice were administered CPT-loaded PLA-HPG NPs (n=7), PLA-

HPG-Ad NPs (n=5), free CPT (n=5), and PBS (n=5) at 10 mg/kg on days 5, 10, and 15 days post tumor inoculation. BALB/c mice at 8 weeks of age (Charles River) without tumors were also administered doses of both CPT-loaded PLA-HPG (n=4) and PLA-HPG-Ad (n=4) following the same dosing schedule to examine NP toxicity. In both studies, animals were monitored and sacrificed as deemed humanely necessary according to protocols approved by the Yale IACUC. Kaplan-Meier survival curves were plotted and differences in survival between groups was analyzed by a log-rank (Mantel-Cox) test, a Logrank test for trend, and a Gehan-Breslow-Wilcoxon test.

Results

PLGA-DSPE-PEG NP Fabrication and Characterization

We first investigated surface modification of our PLGA NPs with ligands previously suggested to enhance BBB penetration (Figure 1A). NPs were fabricated with increasing amounts of surface-bound ligand; DPSE-PEG-FITC was used to measure density of surface bound PEG. The PLGA-DSPE-PEG surface modified-NPs exhibited a smooth, spherical morphology by SEM (Figure 2); sizing analysis indicated diameters under 100 nm (Table 1). As the amount of ligand added during fabrication increased, ligand density increased on the NP surface (Table 2). Although total ligand density on the NP surface improved with increasing ligand addition, the, efficiency of incorporation decreased from 31% at 1 nmol ligand per mg polymer to 9% at higher concentrations. Using 15 nmol ligand per mg polymer, a maximum of ~400 ligands per NP was observed, resulting in 6.2% NP surface coverage. Despite the increase in surface coverage, increasing the amount of DSPE-PEG in the emulsion step did not alter the encapsulation of nile red, a hydrophobic fluorophore (Table 1). For subsequent work, 10 nmol DSPE-PEG per mg polymer was used to maximize surface coverage and minimize ligand loss during fabrication.

PLGA-DSPE-PEG NPs were fabricated with RVG (as well as control peptide RVMAT, a rabies virus matrix protein fragment) and TGN conjugated to the DSPE-PEG as well as DSPE-mPEG (Figure 3). Spherical NPs of ~100 nm diameter were produced (Table 3). DLS analysis of the hydrodynamic diameter demonstrated hydrated NP size of ~200 nm, comparable to our previously published results with unmodified NPs (5). Addition of DSPE-mPEG and ligands led to zeta potentials that were more positive than unmodified NPs.

PLA-HPG NP Fabrication and Characterization

We conjugated adenosine to hydroxyl groups on the surface of nile red-loaded PLA-HPG to produce PLA-HPG-Ad (Figure 1B). PLA-HPG-Ad NPs were formed with increasing concentrations of Ad (1, 5, and 10%) to test if differences could be observed with targeting ligand density. Conjugation of Ad to the PLA-HPG polymer was confirmed with NMR spectroscopy, which indicated 2.2 Ad molecules per PLA molecule (Figure 4). DLS sizing and zeta potential of untargeted PLA-HPG NPs indicated NPs of diameter 82 ± 41 nm with a zeta potential of −12 mV. PLA-HPG-Ad high-density NPs were similar in size (92 nm ± 27) and zeta potential (−8.3 mV).

In vivo brain uptake of NPs after intravenous injection

Unmodified and modified fluorescently-labeled PLGA-DSPE-PEG and PLA-HPG NPs were injected intravenously via the tail vein. After allowing for NP circulation, total NP uptake was determined by quantification of the fluorophore concentration in brain tissue (Figure 5). For unmodified PLGA NPs, accumulation increased from ~0.1% of injected dose at 2 h (Figure 5A), to 0.3% of injected dose at 4 h (Figure 5B). No additional accumulation was observed at circulation times greater than 4 h (data not shown). In separate experiments, we determined that less than 3% of the fluorophore was released from the NPs during an incubation period of 6 days, confirming that the presence of fluorophore in the brain indicates the presence of NPs. We also confirmed that there was no detectable difference between uptake in brains of normal animals, and those with an intracranial tumor of substantial volume (Supplemental Figure 1), suggesting that our studies in normal animals are predictive for uptake into tumors, as well.

Addition of DSPE-PEG-RVG or DSPE-PEG-RVMAT to the surface of PLGA NPs produced no increase in accumulation of NPs in the brain (Figure 5A). In contrast, PLGA-DSPE-PEG-TGN NPs exhibited uptake that was significantly higher than unmodified PLGA NPs and PLGA-DSPE-mPEG-NPs (although the difference between PLGA-DSPE-mPEG and PLGA-DSPE-PEG-TGN was not statistically significant) (Figure 5B).

PLA-HPG showed significantly higher uptake than PLGA-DSPE-PEG NPs after 4 h of circulation (Figure 5B). Moreover, modification of the PLA-HPG NPs with an adenosine mimic provided further increase in brain uptake. More importantly, the density of adenosine had a significant effect on accumulation of NPs in the brain as increasing the Ad content from 1% to 10% nearly doubled brain uptake (Figure 5B). Extended circulation (24 h) of PLA-HPG and PLA-HPG-Ad NPs led to similar levels of accumulation compared to short circulation (4 h, Figure 5C). Based on these results, the PLA-HPG and the PLA-HPG-Ad-NPs with 10% Ad content were selected for further study.

PLA-HPG-NPs for controlled release of CPT

To determine if PLA-HPG NPs can be used to deliver a chemotherapy drug, we formulated NPs encapsulating CPT, a topoisomerase I inhibitor. PLA-HPG and PLA-HPG-Ad NPs were loaded with CPT with 53% and 58% encapsulation efficiency and 7.8% and 5.9% loading, respectively. CPT-loaded NPs were 140 ± 38 nm (PLA-HPG) and 131 ± 54 nm (PLA-HPG-Ad) in diameter as measured by DLS, with zeta potentials of −23.7mV for PLA-HPG and −18.3 mV for PLA-HPG-Ad. TEM revealed spherical particles of small size (Figure 6A and B). When the NPs were incubated in buffered saline solutions, an initial burst of CPT release lasting about 24 h was observed, followed by several days of near linear release (Figure 6C).

Development and *in vitro* characterization of PLA-HPG-Ad NPs

Coumarin 6-loaded PLA-HPG and PLA-HPG-Ad NPs were incubated with bEnd.3 immortalized mouse brain endothelial cells and analyzed using confocal microscopy (Figure 7). NP internalization was enhanced in cells treated with PLA-HPG-Ad NPs at both 4 and 24 h, compared to PLA-HPG.

In vitro cytotoxicity assays were performed with both U87 and bEnd.3 cell lines (Figure 8). CPT-NPs showed a similar toxicity in U87 cells when compared to free drug: IC_{50} [Free Drug] = 2.1 μM; IC_{50} [PLA-HPG] = 2.1 μM; IC_{50} [PLA-HPG-Ad] = 1.7 μM (Figure 8A). Toxicity to endothelial cells required about a 10-fold higher drug dose, with the CPT-loaded NPs being more toxic than the free drug: IC_{50} [Free Drug] = 27.1 μM; IC_{50} [PLA-HPG] = 11.1 μM; IC_{50} [PLA-HPG-Ad] = 11.3 μM (Figure 8B).

In vivo survival analysis of PLA-HPG and PLA-HPG-Ad CPT loaded NPs

To test the therapeutic potential of NPs delivered through the BBB, human immortalized U87 tumors were inoculated in the striatum of athymic nude mice. Three days post-surgery, animals were administered either CPT-loaded PLA-HPG or PLA-HPG-Ad NPs or controls via the tail vein at 4mg/kg CPT. Two additional treatments were administered at day 6 and 9. Mice were monitored and sacrificed as deemed humanely necessary. At the termination of the study, no survival benefit was observed with therapeutic NPs at this chemotherapeutic dose and treatment regimen (Figure 9A). Median survival times were calculated at 34 days for PBS and CPT-loaded HPG-PLA CPT treatments, 35 days for CPT-loaded HPG-PLA-Ad treatment, and 37.5 days for Free CPT. To determine if a higher dose of NPs would be tolerated and effective, a second survival study was performed with injections of 10 mg/kg at days 5, 10, and 15 days post tumor inoculation. No benefit in survival was observed (median survival: 36 days PBS, 35 days Free CPT, 32 days PLA-HPG CPT and PLA-HPG-Ad CPT, Figure 9B). This higher dose (10 mg/kg) appeared to be the maximum tolerable dose, as some athymic nude mice were found to develop adverse reactions (possible arrhythmias) following the injection. Of note, these reactions were not observed in BALB/c mice injected with the same dose of CPT-loaded PLA-HPG-Ad NPs. PLA-HPG NPs did not produce any observable toxic effects when administered at the same dose in both nude and BALB/c mice.

Discussion

Polymer NPs are popular vehicles for delivery across the BBB (15, 53–55). In recent years, surface modification of NPs with ligands intended to increase systemic circulation and permeation through the BBB has become a popular strategy for enhancing accumulation of NPs in the brain (15, 54, 56), although quantitative descriptions of NP uptake in the brain are rare. In this study, we examined 100-nm diameter, brain-targeted, degradable polymer NPs as potential vehicles for overcoming the BBB. Significant differences in NP uptake into the brain were observed, particularly for degradable NPs composed of PLA and HPG (Figure 5). Overall, our optimization of NP design led to an eight-fold increase in brain uptake from ~0.1% of injected dose (for PLGA NPs) to ~0.8% of injected dose (for PLA-HPG-Ad NPs).

In prior work, we showed that PLGA-DSPE-PEG NPs (PLGA NPs with amphiphilic DSPE-PEG assembled on the particle surface) provide high loading of drugs and controlled release (51). We have also shown that PLA-HPG NPs, which have a highly branched polyglycerol surface, provide extended circulation after intravenous injection when compared to PLA-PEG NPs (30). HPG coating provides several advantages over PEG coating, including an extended systemic circulation, which is important to allow the NPs to interact with the BBB (57). Moreover, although PEG has been shown to reduce immunogenicity of certain

macromolecules (58), anti-PEG immune responses have been observed when PEGylated nanomedicines were repeatedly injected (59); the production of anti-PEG IgM was associated with accelerated blood clearance. Thus the use of alternative coating strategies—such as the branched, unstructured HPG we use here—could avoid this immune response.

Targeting to brain endothelial cell surface receptors has been tested by coupling ligands directed against these receptors to the external surface of NPs (15, 16, 60–63). For the present studies, targeting ligands were selected based on their potential for BBB uptake in prior reports (15, 16, 42–45, 47, 48, 64). In our work, PLGA-DSPE-PEG NPs conjugated with RVG or the control peptide RVMAT did not lead to increased accumulation of NPs in the brain. In contrast, the addition of DSPE-mPEG or DSPE-PEG-TGN significantly increased uptake over unmodified NPs. In a previous report, PLGA-PEG NPs modified with different concentrations of TGN peptide showed high amounts of brain uptake that increased with added TGN, although the density of TGN on the final NP preparation was not reported (15).

PLA-HPG-Ad NPs were found to produce significantly higher amounts of brain uptake than any of the alternate NPs tested *in vivo*. In addition, higher uptake was observed at both 4 and 24 h after IV injection, indicating that NPs are either retained in the brain or that there is sustained NP uptake of these long-circulating NPs. Most reports of successful NP BBB delivery indicate a transient influx of brain uptake within the first few hours after administration, with decreasing levels in the brain measured over time (15, 16). The sustained retention in the parenchyma provided by PLA-HPG could potentially enhance the therapeutic potential of these NPs, providing for increased and sustained release of drugs, such as CPT, in the local brain environment. Adenosine is thought to cross the blood-brain barrier by carrier-mediated transport through the concentrative nucleoside transporter type 2 (CNT2) on the endothelial cell surface (65, 66). In addition, adenosine has been found to bind G-protein coupled receptors A_1, A_{2A}, A_{2B}, and A_3 on different cells in the body (67). Recent studies also suggest that engagement of A_{2A} on blood-brain barrier may produce a transient and controlled opening of the BBB (47). In previous work, this transient BBB opening has provided a pathway for macromolecules, such as dextran, to enter the brain parenchyma (16, 47). For example, a previous study showed that Ad conjugated to PAMAM dendrimers was able to enhance BBB permeability through A_{2A} receptor binding, providing a therapeutic window in which drugs can bypass the BBB (16). It is possible that adenosine works in a similar mode here, allowing entry of our drug-loaded polymeric particles. However, we cannot eliminate the possibility of endocytosis/transcytosis after adenosine receptor binding. It is possible that our NPs may be both activating the receptor and crossing the BBB through this mechanism, though more study is needed to confirm this hypothesis.

PLGA-DSPE-PEG and PLA-HPG NPs were shown to increase brain uptake even without an additional targeting ligand, with PLA-HPG NPs producing more accumulation than PLGA-DSPE-PEG NPs. Although no mechanism of specific uptake has yet been deciphered for DSPE-PEG, HPG, or other PEG motifs, PEGylation has been shown to increase BBB uptake of polymeric NPs in mice with intracranial tumors, which was attributed to diffusion and/or convection across the blood-tumor barrier (68).

In our *in vivo* study, the percent dose recovered from normal brain tissue for our best NP formulation was ~1% of total dose administered, which is comparable to the best results that have been previously reported (17, 55). Other studies have observed small differences in uptake in regions of the brain affected by tumors: one recent study using gold-siRNA NPs delivered systemically to mice reported a maximum accumulation of 1% in U87 tumor tissue, with lower amounts in normal brain tissue (17) while another recent study using PLGA NPs found enhanced accumulation of NP-associated fluorescence in the tumor compared to the peritumoral and normal brain regions (53). In our measurements, even in animals with large tumor burdens, we observed no difference in total particle accumulation in tumor-bearing brains (Supplemental Figure 1). Our results suggest that NPs can be optimized to enhance accumulation in the brain, but there are limitations to the number of particles that can enter the brain. In fact, all evidence published to date suggests a limit of ~1% of injected dose: it is not clear if this level of uptake will provide for effective therapy in the brain nor whether the side effects in other tissues will be tolerable.

Other studies using similar strategies (although different targeting ligands and agents) have reported significant, but modest, improvements in median survival in mice with intracranial tumors (31, 64, 69). Dual targeted docetaxel-loaded PEG-PCL NPs—coated with TGN as well as a glioma targeted aptamer—increased mean survival in mice with C6 glioma from 17 to 32 days as compared to unmodified NPs, while survival with NPs presenting only the TGN peptide were not statistically different than untargeted NP controls (64). In mice with U87 tumors, paclitaxel-loaded polycaprolactone NPs conjugated to Angiopep, a peptide thought to target the low density lipoprotein receptor related protein, increased median survival from 30 to 37 days compared to untargeted NPs (31). In mice with U87 glioma, siRNA-coated gold NPs were found to statistically increase the survival compared to controls (17). Although these studies have shown the potential of the approach, the absence of long-term survivors is notable.

To be effective as a treatment for glioblastoma, NPs must be designed to deliver drugs to the brain at therapeutically relevant concentrations. Due to low overall uptake of NPs into the brain, NPs must have high drug loadings to be effective. CPT, which has been shown to be effective against glioma *in vitro* and *in vivo* (23, 53, 70, 71), was readily encapsulated in our PLA-HPG and PLA-HPG-Ad NPs; these particles exhibit sustained release and cytotoxicity in U87 cells (Figure 8A). In addition, *in vivo* retention was observed 24 h after a single IV dose (Figure 5C). However, when delivered at the maximally tolerated dose in an i*n vivo* survival study in mice with intracranial U87 tumors, these NPs did not show any survival benefit (Figure 9B). However, given the promising characteristics observed in our studies with PLA-HPG-Ad NPs, encapsulation of more potent agents (CPT is not particularly potent, with an IC50 of ~1 μM, Figure 8A), perhaps in other disease settings, should be explored.

An alternate approach for NP administration—using direct delivery of drug-loaded polymer NPs into the brain via convection-enhanced delivery (CED) (5, 22)—provides an interesting point of comparison. In CED of NPs, a catheter is inserted into the brain, and a suspension of polymeric NPs is infused into the tissue, providing widespread local distribution and subsequent controlled release of drug from the NPs. From previous results with CED, we

estimate that the maximum dose that could be administered to a mouse is ~0.25 mg CPT, or roughly half the dose delivered in NPs by CED to rats (22, 72). In our present study, assuming that 1% of NPs accumulate at the tumor site at the highest therapeutic dose delivered systemically (10 mg/kg or 0.2 mg CPT for a 20 g mouse), only 2 μg of CPT in NPs is delivered to the brain. Therefore, CED provides about 100-fold higher drug dose to the brain, compared to even the best IV administered NP preparations. This could explain the more significant increases in survival that are observed with CED delivery of NPs, compared to IV-administered NPs designed to cross the BBB.

Conclusions

Polymeric NPs are interesting potential delivery vehicles for neurodegenerative diseases and brain tumors. Importantly, the drug delivery properties of NPs can be enhanced by adding elements to extend systemic circulation and improve transport through the BBB. In this study we tested two different polymeric NPs, which were surface modified to increase circulation time and modified with ligands to increase BBB penetration. Our results indicate that encapsulation of drugs within PLA-HPG-Ad NPs is a promising approach for increasing BBB uptake. These NPs were found to increase brain accumulation after intravenous injection, outperforming other NP designs. Although these NPs were not successful for treatment of intracranial tumors in our initial tests, our results indicate that the high-density HPG coating, which allows for high density conjugation of targeting ligands and as well as high drug loading, is potentially useful for delivery of agents across the BBB.

Supplementary Material

Refer to Web version on PubMed Central for supplementary material.

Acknowledgements

We are grateful to Dr. Andrew Sawyer and Dr. Alice Gaudin for their helpful discussions and thoughtful comments.

This work was supported by the US National Institutes of Health through grants from the National Cancer Institute (R01-CA154460) and the National Center for Advancing Translational Sciences of the National Institutes of Health Grant (TL1-TR000141). In addition, this material is based upon work supported by the National Science Foundation Graduate Research Fellowship Program (DGE-1122492).

References

1. Mayberg M, Langer RS, Zervas NT, Moskowitz MA. Perivascular meningeal projections from cat trigeminal ganglia: possible pathway for vascular headaches in man. Science. 1981; 213(4504):228–30. [PubMed: 6166046]
2. During MJ, Freese A, Sabel BA, Saltzman WM, Deutch A, Roth RH, et al. Controlled release of dopamine from a polymeric brain implant: in vivo characterization. Annals of neurology. 1989; 25(4):351–6. [PubMed: 2634975]
3. Freese A, Sabel BA, Saltzman WM, During MJ, Langer R. Controlled release of dopamine from a polymeric brain implant: in vitro characterization. Exp Neurol. 1989; 103(3):234–8. [PubMed: 2920789]
4. Fung LK, Ewend MG, Sills A, Sipos EP, Thompson R, Watts M, et al. Pharmacokinetics of interstitial delivery of carmustine, 4-hydroperoxycyclophosphamide, and paclitaxel from a biodegradable polymer implant in the monkey brain. Cancer research. 1998; 58(4):672–84. [PubMed: 9485020]

5. Zhou J, Patel TR, Sirianni RW, Strohbehn G, Zheng MQ, Duong N, et al. Highly penetrative, drug-loaded nanocarriers improve treatment of glioblastoma. Proceedings of the National Academy of Sciences of the United States of America. 2013; 110(29):11751–6. [PubMed: 23818631]
6. Barchet TM, Amiji MM. Challenges and opportunities in CNS delivery of therapeutics for neurodegenerative diseases. Expert Opin Drug Deliv. 2009; 6(3):211–25. [PubMed: 19290842]
7. Institute NC. SEER Stat Fact Sheets: Brain and Other Nervous System Cancer. 2015. Available from: http://seer.cancer.gov/statfacts/html/brain.html#risk
8. Weller M, Cloughesy T, Perry JR, Wick W. Standards of care for treatment of recurrent glioblastoma--are we there yet? Neuro Oncol. 2013; 15(1):4–27. [PubMed: 23136223]
9. Stupp R, Mason WP, van den Bent MJ, Weller M, Fisher B, Taphoorn MJB, et al. Radiotherapy plus concomitant and adjuvant temozolomide for glioblastoma. New Engl J Med. 2005; 352(10):987–96. [PubMed: 15758009]
10. Johnson DR, O'Neill BP. Glioblastoma survival in the United States before and during the temozolomide era. J Neuro-Oncol. 2012; 107(2):359–64.
11. Pardridge WM. Drug transport across the blood-brain barrier. Journal of cerebral blood flow and metabolism : official journal of the International Society of Cerebral Blood Flow and Metabolism. 2012; 32(11):1959–72.
12. Abbott NJ, Patabendige AA, Dolman DE, Yusof SR, Begley DJ. Structure and function of the blood-brain barrier. Neurobiol Dis. 2010; 37(1):13–25. [PubMed: 19664713]
13. van Tellingen, O.; Yetkin-Arik, B.; de Gooijer, MC.; Wesseling, P.; Wurdinger, T.; de Vries, HE. Drug resistance updates : reviews and commentaries in antimicrobial and anticancer chemotherapy. 2015. Overcoming the blood-brain tumor barrier for effective glioblastoma treatment.
14. Lockman PR, Mittapalli RK, Taskar KS, Rudraraju V, Gril B, Bohn KA, et al. Heterogeneous blood-tumor barrier permeability determines drug efficacy in experimental brain metastases of breast cancer. Clinical cancer research : an official journal of the American Association for Cancer Research. 2010; 16(23):5664–78. [PubMed: 20829328]
15. Li J, Feng L, Fan L, Zha Y, Guo L, Zhang Q, et al. Targeting the brain with PEG-PLGA nanoparticles modified with phage-displayed peptides. Biomaterials. 2011; 32(21):4943–50. [PubMed: 21470674]
16. Gao X, Qian J, Zheng S, Changyi Y, Zhang J, Ju S, et al. Overcoming the blood-brain barrier for delivering drugs into the brain by using adenosine receptor nanoagonist. ACS Nano. 2014; 8(4): 3678–89. [PubMed: 24673594]
17. Jensen SA, Day ES, Ko CH, Hurley LA, Luciano JP, Kouri FM, et al. Spherical Nucleic Acid Nanoparticle Conjugates as an RNAi-Based Therapy for Glioblastoma. Science translational medicine. 2013; 5(209)
18. Cheng CJ, Tietjen GT, Saucier-Sawyer JK, Saltzman WM. A holistic approach to targeting disease with polymeric nanoparticles. Nat Rev Drug Discov. 2015; 14(4):239–47. [PubMed: 25598505]
19. Marin E, Briceno MI, Caballero-George C. Critical evaluation of biodegradable polymers used in nanodrugs. International journal of nanomedicine. 2013; 8:3071–91. [PubMed: 23990720]
20. Shive MS, Anderson JM. Biodegradation and biocompatibility of PLA and PLGA microspheres. Advanced drug delivery reviews. 1997; 28(1):5–24. [PubMed: 10837562]
21. Woodrow KA, Cu Y, Booth CJ, Saucier-Sawyer JK, Wood MJ, Saltzman WM. Intravaginal gene silencing using biodegradable polymer nanoparticles densely loaded with small-interfering RNA. Nat Mater. 2009; 8(6):526–33. [PubMed: 19404239]
22. Sawyer AJ, Saucier-Sawyer JK, Booth CJ, Liu J, Patel T, Piepmeier JM, Saltzman WM. Convection-enhanced delivery of camptothecin-loaded polymer nanoparticles for treatment of intracranial tumors. Drug delivery and translational research. 2011; (1):34–42. [PubMed: 21691426]
23. Ediriwickrema A, Zhou J, Deng Y, Saltzman WM. Multi-layered nanoparticles for combination gene and drug delivery to tumors. Biomaterials. 2014; 35(34):9343–54. [PubMed: 25112935]
24. Zhou J, Patel TR, Fu M, Bertram JP, Saltzman WM. Octa-functional PLGA nanoparticles for targeted and efficient siRNA delivery to tumors. Biomaterials. 2012; 33(2):583–91. [PubMed: 22014944]

25. Cheng J, Teply BA, Sherifi I, Sung J, Luther G, Gu FX, et al. Formulation of functionalized PLGA-PEG nanoparticles for in vivo targeted drug delivery. Biomaterials. 2007; 28(5):869–76. [PubMed: 17055572]
26. Park J, Fong PM, Lu J, Russell KS, Booth CJ, Saltzman WM, et al. PEGylated PLGA nanoparticles for the improved delivery of doxorubicin. Nanomedicine. 2009; 5(4):410–8. [PubMed: 19341815]
27. Chan JM, Zhang L, Yuet KP, Liao G, Rhee JW, Langer R, et al. PLGA-lecithin-PEG core-shell nanoparticles for controlled drug delivery. Biomaterials. 2009; 30(8):1627–34. [PubMed: 19111339]
28. Gref R, Minamitake Y, Peracchia MT, Trubetskoy V, Torchilin V, Langer R. Biodegradable long-circulating polymeric nanospheres. Science. 1994; 263(5153):1600–3. [PubMed: 8128245]
29. Nance EA, Woodworth GF, Sailor KA, Shih TY, Xu Q, Swaminathan G, et al. A dense poly(ethylene glycol) coating improves penetration of large polymeric nanoparticles within brain tissue. Science translational medicine. 2012; 4(149):149ra19.
30. Deng Y, Saucier-Sawyer JK, Hoimes CJ, Zhang J, Seo YE, Andrejecsk JW, et al. The effect of hyperbranched polyglycerol coatings on drug delivery using degradable polymer nanoparticles. Biomaterials. 2014
31. Xin HL, Sha XY, Jiang XY, Zhang W, Chen LC, Fang XL. Anti-glioblastoma efficacy and safety of paclitaxel-loading Angiopep-conjugated dual targeting PEG-PCL nanoparticles. Biomaterials. 2012; 33(32):8167–76. [PubMed: 22889488]
32. Ulbrich K, Knobloch T, Kreuter J. Targeting the insulin receptor: nanoparticles for drug delivery across the blood-brain barrier (BBB). Journal of Drug Targeting. 2011; 19(2):125–32. [PubMed: 20387992]
33. Jain A, Chasoo G, Singh SK, Saxena AK, Jain SK. Transferrin-appended PEGylated nanoparticles for temozolomide delivery to brain: in vitro characterisation. J Microencapsul. 28(1):21–8. [PubMed: 21171813]
34. Bickel U, Yoshikawa T, Pardridge WM. Delivery of peptides and proteins through the blood-brain barrier. Advanced drug delivery reviews. 2001; 46(1–3):247–79. [PubMed: 11259843]
35. Herve F, Ghinea N, Scherrmann JM. CNS delivery via adsorptive transcytosis. Aaps J. 2008; 10(3): 455–72. [PubMed: 18726697]
36. Liu L, Guo K, Lu J, Venkatraman SS, Luo D, Ng KC, et al. Biologically active core/shell nanoparticles self-assembled from cholesterol-terminated PEG-TAT for drug delivery across the blood-brain barrier. Biomaterials. 2008; 29(10):1509–17. [PubMed: 18155137]
37. Abbott NJ, Patabendige AA, Dolman DE, Yusof SR, Begley DJ. Structure and function of the blood-brain barrier. Neurobiol Dis. 37(1):13–25. [PubMed: 19664713]
38. Ulbrich K, Knobloch T, Kreuter J. Targeting the insulin receptor: nanoparticles for drug delivery across the blood-brain barrier (BBB). J Drug Target. 19(2):125–32. [PubMed: 20387992]
39. Smith MW, Gumbleton M. Endocytosis at the blood-brain barrier: from basic understanding to drug delivery strategies. J Drug Target. 2006; 14(4):191–214. [PubMed: 16777679]
40. Lafon M. Rabies virus receptors. J Neurovirol. 2005; 11(1):82–7. [PubMed: 15804965]
41. Lentz TL, Burrage TG, Smith AL, Tignor GH. The acetylcholine receptor as a cellular receptor for rabies virus. Yale J Biol Med. 1983; 56(4):315–22. [PubMed: 6367238]
42. Kumar P, Wu H, McBride JL, Jung KE, Kim MH, Davidson BL, et al. Transvascular delivery of small interfering RNA to the central nervous system. Nature. 2007; 448(7149):39–43. [PubMed: 17572664]
43. Liu Y, Huang R, Han L, Ke W, Shao K, Ye L, et al. Brain-targeting gene delivery and cellular internalization mechanisms for modified rabies virus glycoprotein RVG29 nanoparticles. Biomaterials. 2009; 30(25):4195–202. [PubMed: 19467700]
44. Xiang L, Zhou R, Fu A, Xu X, Huang Y, Hu C. Targeted delivery of large fusion protein into hippocampal neurons by systemic administration. J Drug Target.
45. Park TE, Singh B, Li H, Lee JY, Kang SK, Choi YJ, et al. Enhanced BBB permeability of osmotically active poly(mannitol-co-PEI) modified with rabies virus glycoprotein via selective stimulation of caveolar endocytosis for RNAi therapeutics in Alzheimer's disease. Biomaterials. 2015; 38:61–71. [PubMed: 25457984]

46. Gaudin A, Yemisci M, Eroglu H, Lepetre-Mouelhi S, Turkoglu OF, Donmez-Demir B, et al. Squalenoyl adenosine nanoparticles provide neuroprotection after stroke and spinal cord injury. Nature nanotechnology. 2014; 9(12):1054–62.
47. Carman AJ, Mills JH, Krenz A, Kim DG, Bynoe MS. Adenosine receptor signaling modulates permeability of the blood-brain barrier. The Journal of neuroscience : the official journal of the Society for Neuroscience. 2011; 31(37):13272–80. [PubMed: 21917810]
48. Kim, DG.; Bynoe, MS. Molecular neurobiology. 2014. A2A Adenosine Receptor Regulates the Human Blood-Brain Barrier Permeability.
49. Thorne RG, Nicholson C. In vivo diffusion analysis with quantum dots and dextrans predicts the width of brain extracellular space. Proceedings of the National Academy of Sciences of the United States of America. 2006; 103(14):5567–72. [PubMed: 16567637]
50. Hobbs SK, Monsky WL, Yuan F, Roberts WG, Griffith L, Torchilin VP, et al. Regulation of transport pathways in tumor vessels: role of tumor type and microenvironment. Proceedings of the National Academy of Sciences of the United States of America. 1998; 95(8):4607–12. [PubMed: 9539785]
51. Cheng CJ, Saltzman WM. Enhanced siRNA delivery into cells by exploiting the synergy between targeting ligands and cell-penetrating peptides. Biomaterials. 2011; 32(26):6194–203. [PubMed: 21664689]
52. Vauthier C, Schmidt C, Couvreur P. Measurement of the density of polymeric nanoparticulate drug carriers by isopycnic centrifugation. J Nanopart Res. 1999; 1(3):411–8.
53. Householder KT, DiPerna DM, Chung EP, Wohlleb GM, Dhruv HD, Berens ME, et al. Intravenous delivery of camptothecin-loaded PLGA nanoparticles for the treatment of intracranial glioma. Int J Pharm. 2015; 479(2):374–80. [PubMed: 25562639]
54. Xin HL, Sha XY, Jiang XY, Chen LC, Law K, Gu JJ, et al. The brain targeting mechanism of Angiopep-conjugated poly(ethylene glycol)-co-poly(epsilon-caprolactone) nanoparticles. Biomaterials. 2012; 33(5):1673–81. [PubMed: 22133551]
55. Kreuter J. Drug delivery to the central nervous system by polymeric nanoparticles: what do we know? Advanced drug delivery reviews. 2014; 71:2–14. [PubMed: 23981489]
56. Xin HL, Jiang XY, Gu JJ, Sha XY, Chen LC, Law K, et al. Angiopep-conjugated poly(ethylene glycol)-co-poly(epsilon-caprolactone) nanoparticles as dual-targeting drug delivery system for brain glioma. Biomaterials. 2011; 32(18):4293–305. [PubMed: 21427009]
57. Alavijeh MS, Palmer AM. Measurement of the pharmacokinetics and pharmacodynamics of neuroactive compounds. Neurobiol Dis. 2010; 37(1):38–47. [PubMed: 19818851]
58. Harris JM, Chess RB. Effect of pegylation on pharmaceuticals. Nat Rev Drug Discov. 2003; 2(3): 214–21. [PubMed: 12612647]
59. Saadati R, Dadashzadeh S, Abbasian Z, Soleimanjahi H. Accelerated blood clearance of PEGylated PLGA nanoparticles following repeated injections: effects of polymer dose, PEG coating, and encapsulated anticancer drug. Pharmaceutical research. 2013; 30(4):985–95. [PubMed: 23184228]
60. Huile G, Shuaiqi P, Zhi Y, Shijie C, Chen C, Xinguo J, et al. A cascade targeting strategy for brain neuroglial cells employing nanoparticles modified with angiopep-2 peptide and EGFP-EGF1 protein. Biomaterials. 2011; 32(33):8669–75. [PubMed: 21843903]
61. Xin H, Jiang X, Gu J, Sha X, Chen L, Law K, et al. Angiopep-conjugated poly(ethylene glycol)-co-poly(epsilon-caprolactone) nanoparticles as dual-targeting drug delivery system for brain glioma. Biomaterials. 32(18):4293–305. [PubMed: 21427009]
62. Gao H, Zhang S, Cao S, Yang Z, Pang Z, Jiang X. Angiopep-2 and activatable cell-penetrating peptide dual-functionalized nanoparticles for systemic glioma-targeting delivery. Molecular pharmaceutics. 2014; 11(8):2755–63. [PubMed: 24983928]
63. Cui Y, Xu Q, Chow PK, Wang D, Wang CH. Transferrin-conjugated magnetic silica PLGA nanoparticles loaded with doxorubicin and paclitaxel for brain glioma treatment. Biomaterials. 2013; 34(33):8511–20. [PubMed: 23932498]
64. Gao H, Qian J, Cao S, Yang Z, Pang Z, Pan S, et al. Precise glioma targeting of and penetration by aptamer and peptide dual-functioned nanoparticles. Biomaterials. 2012; 33(20):5115–23. [PubMed: 22484043]

65. Pardridge WM. The blood-brain barrier: bottleneck in brain drug development. NeuroRx. 2005; 2(1):3–14. [PubMed: 15717053]

66. Li JY, Boado RJ, Pardridge WM. Cloned blood-brain barrier adenosine transporter is identical to the rat concentrative Na+ nucleoside cotransporter CNT2. Journal of cerebral blood flow and metabolism : official journal of the International Society of Cerebral Blood Flow and Metabolism. 2001; 21(8):929–36.

67. Jacobson KA, Gao ZG. Adenosine receptors as therapeutic targets. Nat Rev Drug Discov. 2006; 5(3):247–64. [PubMed: 16518376]

68. Brigger I, Morizet J, Aubert G, Chacun H, Terrier-Lacombe MJ, Couvreur P, et al. Poly(ethylene glycol)-coated hexadecylcyanoacrylate nanospheres display a combined effect for brain tumor targeting. Journal of Pharmacology and Experimental Therapeutics. 2002; 303(3):928–36. [PubMed: 12438511]

69. Gu GZ, Gao XL, Hu QY, Kang T, Liu ZY, Jiang MY, et al. The influence of the penetrating peptide iRGD on the effect of paclitaxel-loaded MT1-AF7p-conjugated nanoparticles on glioma cells. Biomaterials. 2013; 34(21):5138–48. [PubMed: 23582684]

70. Sawyer AJ, Saucier-Sawyer JK, Booth CJ, Liu J, Patel T, Piepmeier JM, et al. Convection-enhanced delivery of camptothecin-loaded polymer nanoparticles for treatment of intracranial tumors. Drug delivery and translational research. 2011; 1(1):34–42. [PubMed: 21691426]

71. Chevalier A, Dubois M, Le Joncour V, Dautrey S, Lecointre C, Romieu A, et al. Synthesis, biological evaluation, and in vivo imaging of the first camptothecin-fluorescein conjugate. Bioconjugate chemistry. 2013; 24(7):1119–33. [PubMed: 23750546]

72. Serwer L, Hashizume R, Ozawa T, James CD. Systemic and local drug delivery for treating diseases of the central nervous system in rodent models. Journal of visualized experiments : JoVE. 2010; (42)

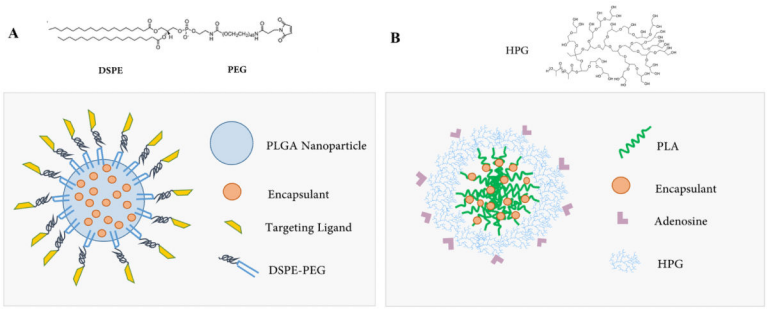

Figure 1.
A) PLGA-DSPE-PEG and B) PLA-HPG Targeted NP Structure.

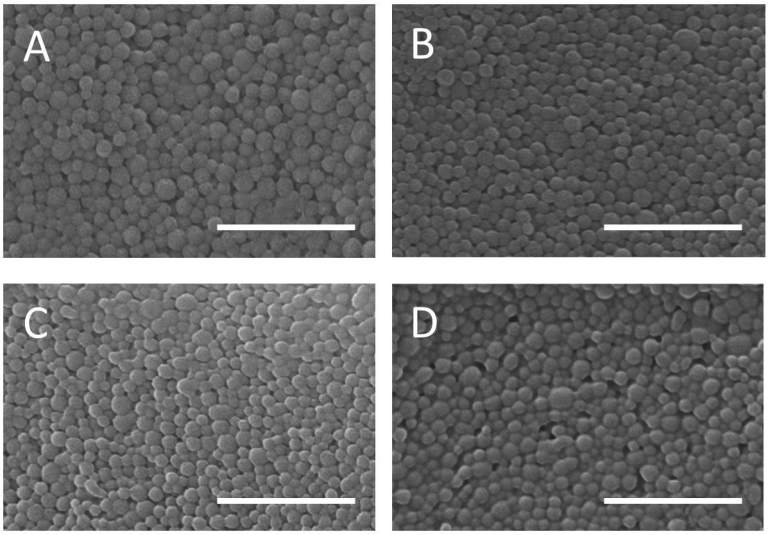

Figure 2.

SEM images of DSPE-PEG-FITC modified PLGA NPs. NPs were fabricated at increasing DSPE-PEG-FITC density to quantify total ligand incorporation at A) 15 nmol/mg, B) 10 nmol/mg, C) 5 nmol/mg, and D) 1 nmol/mg. SEM sizing indicates that increasing ligand concentration during fabrication does not significantly alter NP size. Scale bar = 1 um

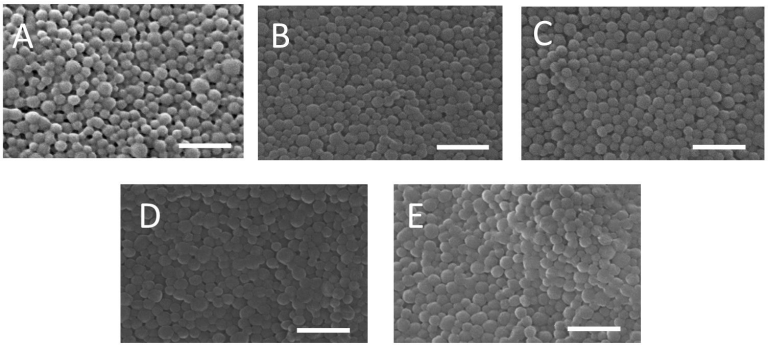

Figure 3.

SEM images of modified and unmodified PLGA-DSPE-PEG NPs. A) Unmodified NPs, B) DSPE-PEG-RVG, C) DSPE-PEG-RVMAT, D) DSPE-mPEG 2000, E) DSPE-PEG-TGN Peptide. Scale bar = 500 nm

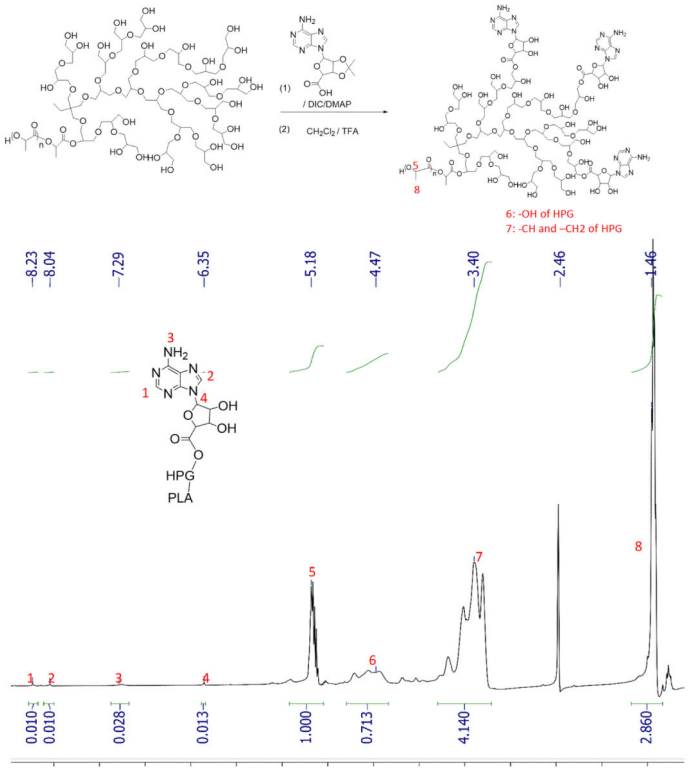

Figure 4.

Structure of PLA-HPG-Ad and analysis by NMR. HPG-PLA was conjugated to Ad as shown. NMR spectra for PLA-HPG-Ad indicates that Ad was effectively conjugated to the PLA-HPG with an average number of 2.2 Ad per PLA.

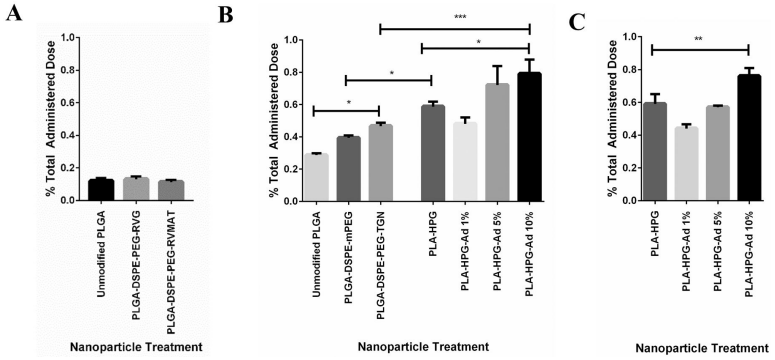

Figure 5.

In vivo accumulation of NPs in brain tissue after intravenous injection. A comparison of the percent injected dose of NPs in homogenized brain samples was performed with A) PLGA-DSPE-PEG-RVG and PLGA-DSPE-PEG-RVMAT at 2h post injection, B) PLGA-DSPE-PEG-TGN and PLA-HPG-Ad at 4 h post injection, and C) PLA-HPG-Ad at 24 h post injection. Highly modified PLA-HPG-Ad produced the highest accumulation in the brain at both 4 and 24 h post infusion and was significantly different than untargeted PLA-HPG at both timepoints (n=4). Significance denoted as * ($p \leq 0.05$), ** ($p \leq 0.01$), *** ($p \leq 0.001$).

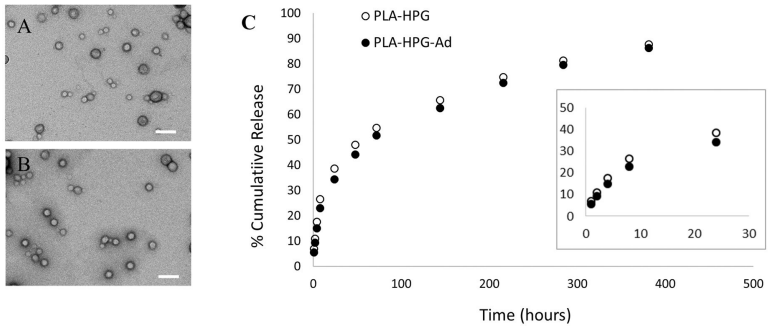

Figure 6.

TEM images and controlled release profiles for CPT-loaded PLA-HPG-Ad and PLA-HPG NPs. TEM images of A) PLA-HPG and B) PLA-HPG-Ad loaded with CPT show spherical particles of small size (Scale bar = 200nm). Controlled release of CPT (C) indicates extended and continuous release of the drug. Inset indicates release during the first 24 hours of incubation.

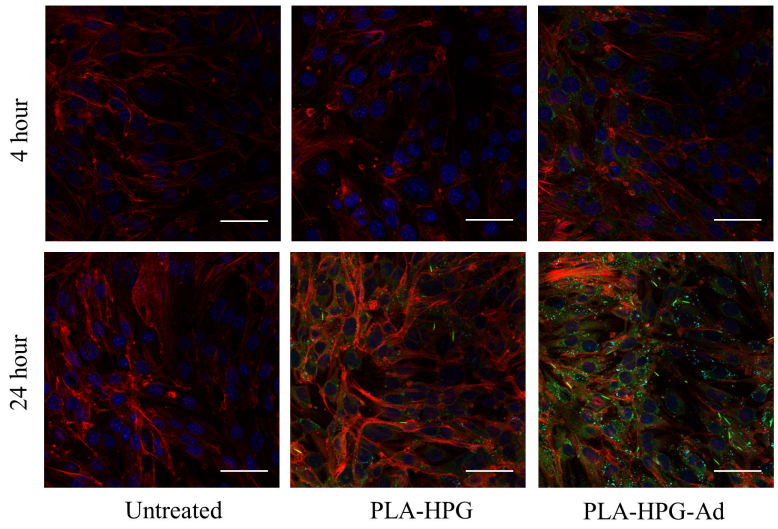

Figure 7.

Confocal microscopy of bEnd.3 cells after incubation with PLA-HPG and PLA-HPG-Ad NPs. Cells were cultured for either 4 or 24 h after addition of NPs. Microscopy showed enhanced uptake of PLA-HPG-Ad NPs at both timepoints as compared to unmodified NPs. Red- actin (phalloidin), green – NPs (coumarin 6), blue-nucleus (DAPI). Scale bar = 50μm

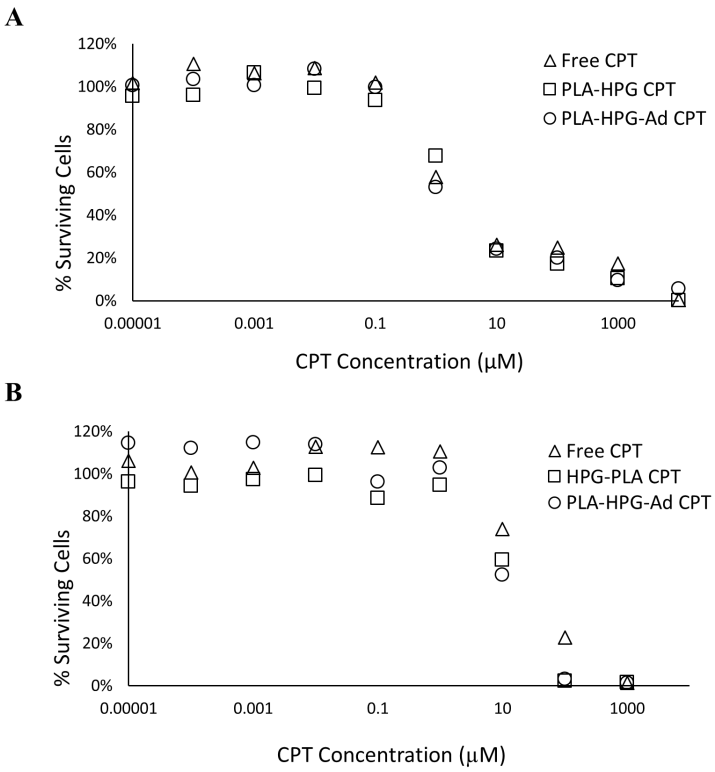

Figure 8.

Cytotoxicity of PLA-HPG and PLA-HPG-Ad NPs loaded with CPT in A) U87 glioblastoma cells and B) bEnd.3 cells. In general, both sets of NPs had similar cytotoxicity against U87 and bEnd.3 cells, which was also similar to free drug. A small increase in cytotoxicity to bEnd.3 cells was observed with CPT NPs.

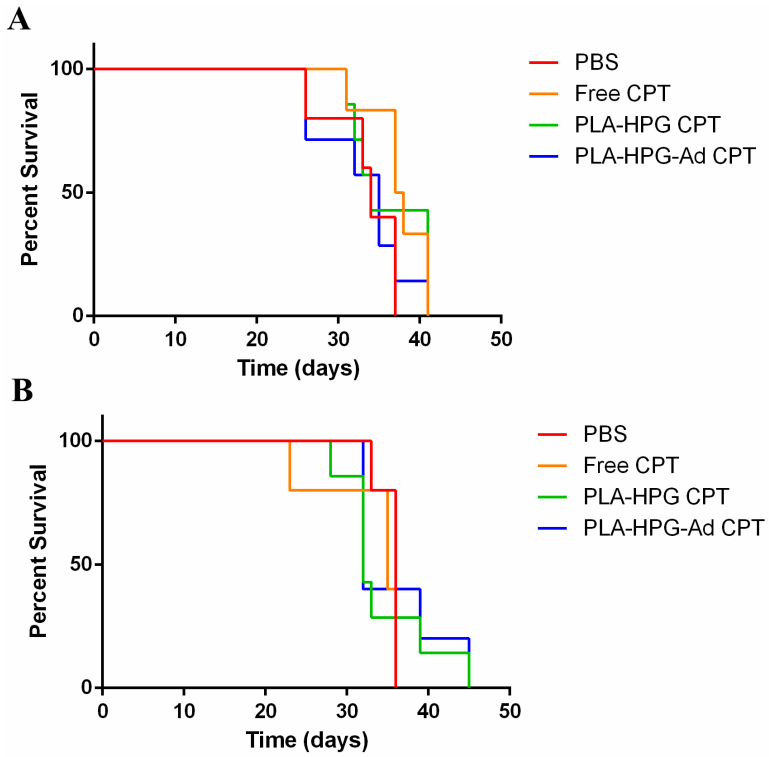

Figure 9.

Kaplan-Meier survival analysis of CPT-loaded adenosine NPs administered via systemic tail vein delivery in mice with intracranial U87 tumors. Particles were administered via the tail vein A) 3 days post tumor inoculation at a CPT concentration of 4 mg/kg in each dose and B) 5 days post tumor inoculation at a CPT concentration of 10 mg/kg at each dose. For A, n=7 (PLA-HPG CPT and PLA-HPG-Ad CPT), n=6 (Free CPT), n=5 (PBS). For B, n=7 (PLA-HPG CPT), n=5 (PLA-HPG-Ad CPT, Free CPT, PBS).

Table 1

Sizing and Encapsulation Efficiency of nile red in DSPE-PEG-FITC NPs

Ligand Concentration During Fabrication (nmol ligand/mg polymer)	Average Diameter, SEM (nm ± SD)	Encapsulation Efficiency (%)
15	93 ± 33	95
10	90 ± 32	91
5	91 ± 29	95
1	95 ± 37	86

Table 2

DSPE-PEG-FITC ligand density and percent incorporation

Ligand Concentration During Fabrication (nmol ligand/mg polymer)	Ligand Concentration post-Fabrication (nmol DSPE-PEG-FITC/mg NPs)	DSPE-PEG Incorporation Efficiency (%)	Ligands per NP	NP Surface Coverage (%)
15	1.3	9	396	6.2
10	0.92	9	254	4.2
5	0.44	9	125	2.0
1	0.31	31	101	1.5

Table 3

DSPE-PEG modified NP sizing and zeta potential analysis

Surface Modification	Average Diameter, SEM (nm ± SD)	Hydrodynamic Diameter, DLS (nm ± SD)	Zeta Potential
Unmodified	92 ± 32	179 ± 52	−17.9
DSPE-PEG-RVG	97 ± 34	196 ± 59	−14.2
DSPE-PEG-RVMAT	95 ± 36	193 ± 64	−14.9
DSPE-mPEG	86 ± 41	185 ± 66	−8.8
DSPE-PEG-TGN	87 ± 47	188 ± 60	−15.3